DOI:10.1021/jf100743z

JOURNAL OF AGRICULTURAL AND FOOD CHEMISTRY
ARTICLE

Effect of Cysteine on Lowering Protein Aggregation and Subsequent Hardening of Whey Protein Isolate (WPI) Protein Bars in WPI/Buffer Model Systems

Dan Zhu and Theodore P. Labuza*

Department of Food Science and Nutrition, University of Minnesota, 1334 Eckles Avenue, St. Paul, Minnesota 55108

Whey protein isolate (WPI) bar hardening without and with cysteine (Cys) or *N*-ethylmaleimide (NEM) was investigated in model systems (WPI/buffer = 6:4, by weight, pH 6.8, $a_w \sim 0.97$) in an accelerated shelf-life test (ASLT) at 45 °C over a period of up to 35 days. The formation of insoluble aggregates as determined by solubility and the structural rearrangement of WPI protein aggregates as observed by SEM were responsible for the WPI bars' hardening. As corroborated by electrophoresis analysis, both β-lactoglobulin (β-lg) and α-lactalbumin (α-la) were involved in the formation of aggregates via the thiol−disulfide interchange reaction and/or noncovalent interactions. The former force dominated the bar hardening at an earlier stage, whereas the latter force played a role for the long-term hardening. In comparison with the control bar without Cys, the thiol−disulfide interchange reaction was significantly reduced by Cys (WPI/Cys = 0.05), increased by Cys (WPI/Cys = 0.25), and inhibited by NEM (WPI/NEM = 2). Therefore, bar hardening was significantly delayed by Cys (WPI/Cys = 0.05) and NEM but accelerated by Cys (WPI/Cys = 0.25).

KEYWORDS: Whey protein isolate; protein bar; hardness; cysteine; shelf life

INTRODUCTION

Protein bars, as modified snack bars, were introduced in the market in the early 1990s. The diversity of protein bars varies widely depending on the functional intent, such as nutrition bars, energy bars, or sports bars aiming at losing weight, benefitting heart health, improving LDL-cholesterol levels, and strengthening muscles (*1*, *2*). However, protein bars suffer from a degradation of quality during storage due to loss of nutritional value, hardening of texture, and deterioration of taste. Among those factors, hardening is the major concern for protein bar manufacturers. Usually, the shelf life of protein bars is 6−9 months at room temperature. The higher the storage temperature, the faster the bar hardens. If a bar is too hard and thus does not taste good, no matter how nutritious or healthy it is, consumers will not buy it. To our knowledge, there has been no report on preventing protein bar hardening.

Typically, commercial protein bars contain about 20−40% protein, 10−50% carbohydrates, and 10−15% fats with a water activity (a_w) of 0.5−0.65. During storage, various physical and chemical reactions occur, for example, water migration, nonenzymatic browning (NEB), lipid oxidation, and protein aggregation. For a whey protein isolate (WPI)/buffer model system, Zhou et al. (*3*, *4*) reported that protein aggregation is responsible for bar hardening through the formation of insoluble aggregates induced by the thiol−disulfide interchange reaction. This led us to hypothesize that if the thiol−disulfide interchange reaction could be prevented, the hardening of the protein bars could be inhibited, resulting in a longer shelf life.

Theoretically, it is not difficult to prevent the thiol−disulfide interchange reaction. For example, Dalgleish et al. (*5*) reported that reducing the pH to ≤6 stops the thiol−disulfide interchange reaction in a 10% WPI protein solution. However, this may or may not take effect in lower a_w systems. The pH (with an initial value of ∼7) of the lower a_w systems generally decreases by ∼1.5 pH units (*6*), which would result in a pH closer to the isoelectric point (p*I* 4.8−5.5) of WPI proteins. If the pH reduces to < 6, the solubility of WPI proteins decreases (*7*). The free thiol group blocking reagents, such as *N*-ethylmaleimide (NEM), 2-iodoacetamide, or iodoacetic acid, or disulfide bond splitters, such as β-mercaptoethanol (2-Me), dithiothreitol, or *p*-chlormercuribenzoate, could efficiently prevent the thiol−disulfide interchange reaction. However, these are toxic and not approved for use in foods in the United States. A promising candidate is L-cysteine hydrochloride (Cys). Cys, a food-grade additive, is allowed in baked foods as a dough strengthener to reduce processing time (21CFR, 184. 1272). The presence of Cys in foods could also produce a meat-like flavor and increase whiteness of the products by reducing the NEB reaction (*8*, *9*). In addition, Cys is one of the popular antioxidants and free radical scavengers in the dietary supplement arena (*10*).

The mechanism of Cys in interfering with the thiol−disulfide interchange reaction in food proteins has been of interest to many researchers. Huggins et al. (*11*) found that Cys is able to cleave disulfide bonds and increase the protein gel strength through the thiol−disulfide interchange reaction. Frendsorff et al. (*12*) observed that the addition of an excess of Cys to serum albumin at

*Author to whom correspondence should be addressed [phone (612) 624-9701; fax (612) 625-5272; e-mail tplabuza@umn.edu].

 Published on Web 06/17/2010 © 2010 American Chemical Society

pH 10 rapidly ruptures most of the intramolecular disulfide cross-links. Because the rupture of disulfide bonds is a reversible reaction, they assumed that if an excess of Cys was added, the aggregation of serum albumin should be prevented. Further studies indicated that the elastic strength of whey protein gel (*13*, *14*), soy protein isolate (*15*), and ovalbumin (*16*) increased with moderate Cys addition, whereas a higher concentration of added Cys drastically reduced the gel strength hardness. By the examination of several globular proteins, Wang and Damodaran (*17*) reported that Cys both cleaved and blocked disulfide bonds and resulted in the unfolding of globular proteins, resulting in a decreased gel strength (hardness). In the making of wheat protein dough, the solubility of wheat protein was increased and the dough hardness was adversely decreased by adding Cys because the extensive disulfide-mediated cross-linking among wheat proteins was weakened by Cys during the extrusion process. The texture of extrudates with 0.25% (w/w) added cysteine had the lowest values for all textural parameters (gumminess, fracturability, cohesiveness, hardness, chewiness, springiness, modulus) (*9*, *18*, *19*).

The major proteins used in commercial nutrition bars include whey protein, soy protein, caseinates, gelatin, hydrolyzed proteins (whey, soy, collagen), and occasionally egg, beef, or rice proteins. We chose WPI, a byproduct of cheesemaking, as the subject in the model systems because it is widely used in protein bars and also because its structure and physicochemical properties have been widely studied. WPI proteins mainly consist of 64% β-lactoglobulin (β-lg), 27% α-lactalbumin (α-la), and 4% bovine serum albumin (BSA) with 5% other constituents including minor proteins, some minerals, and lactose (*20*). The content of lactose in WPI is very low (<1%). This avoids the complexity caused by the NEB reaction between WPI and lactose.

The objective of the present study was to investigate the effect of Cys on lowering protein aggregation and subsequent hardening of WPI protein bars in WPI/buffer model systems stored at 45 °C to accelerate the reaction.

MATERIALS AND METHODS

Materials. The WPI (BiPRO) was kindly provided by Davisco Foods International, Inc. (Eden Prairie, MN). The total amount of protein in the dry base was >97.6%, fat was 0.2%, moisture was 5.0%, and pH was 6.8 (10% solution at 20 °C). Lactose was <1%. Cys (monohydrate, tissue culture grade), sodium phosphate dibasicm and sodium phosphate monobasic, monohydrate 99+% pure (Acros Organics), were purchased from Fisher Scientific. NEM (HPLC grade, ≥99.0%) and 2-Me (99.0%, GC grade) were obtained from Fluka (Sigma-Aldrich, St. Louis, MO). Sodium azide was obtained from Sigma Chemical Co. (St. Louis, MO). Molecular weight standards (Ez-run prestained Rec protein ladder) were purchased from Fisher Scientific (Pittsburgh, PA).

Preparation of WPI Bars in a Model System. WPI powder was mixed with 10 mM sodium phosphate buffer solution (PBS, pH 6.8, and 0.05% sodium azide (NaN_3) to control microbial growth) in a ratio of 3:2 (by weight) at room temperature (23 °C). In the cases when inhibiting reagents were added, the reagents (Cys, NEM) were first dissolved in the PBS buffer. The protein dough was kneaded by hand (with gloves on) as quickly as possible to reduce any loss of moisture. Once the dough formed (all protein powder and water were mixed together until no obvious dry protein powder or liquid buffer was observed, <5 min), replicate samples were then immediately weighed (~9.5 g) and placed into a plastic disposable sample cup (38.5 mm in internal diameter, 11.5 mm in height, Decagon Device, Inc., Pullman, WA). The dough was quickly pressed and evenly distributed in the cup by hand so that the dough had an even flat surface with a height of ~8 mm. The cups were covered with lids and sealed with Parafilm (Pechiney Plastic Packaging, Chicago, IL). The sample cups were then placed into glass jars, which were also sealed by Parafilm around the edges of the lids to avoid moisture loss. After holding at room temperature for 2 h, the sample jars were then stored in an incubator at 45 °C. The samples were taken out at designed time intervals (weekly for 5 weeks), cooled at room temperature for at least 2 h, and then analyzed (3 bar replicates) for all tests.

The molar ratios of reactants for the bars were 0, 0.05, and 0.25 for Cys/WPI and 2 for NEM/WPI. These were chosen on the basis of preliminary experiments of Cys/WPI from 0.0 to 2.7 molar ratio. Corresponding to the molar ratios, the bars in the subsequent tables and figures were defined as Cys0, Cys0.05, Cys0.25, and Nem2, respectively. The average molecular weight of the WPI was ~30400 Da (*21*).

Determination of Water Activity (a_W). The water activity of WPI bars was determined using a water activity meter (AQUA lab model CX-2, Decagon Devices, Inc.).

Texture Analysis. Texture analysis was performed using an SMS TA. XT PLUS Texture Analyzer (Texture Technologies Corp., Scarsdale, NY) with a cylinder probe (P/3 stainless steel, 3 mm in diameter, contact area 7.07 mm^2) at room temperature (23 °C). The test mode was puncture; target mode was distance. The force−distance curves were obtained at a speed of 1.00 mm/s with a distance of 5.00 mm. The force required to penetrate 3 mm into the WPI bars while in the cups was used as an index of the hardness. Two measurements were performed on each of three bars. The force at 3 mm was chosen because according to the instrument manufacturer it essentially eliminates any resistance from the bottom of the cups when the probe is pushed down.

Solubility of Protein Bars in Buffer. WPI bar samples (0.200 g) were dispersed in 30 mL of 10 mM PBS and stirred with a magnetic stirrer on a stirring plate overnight at 5 °C (until all protein bar mass was disrupted into tiny particles with no obvious large grains). The obtained sample suspensions (1.0 mL, 0.67% w/w, using a 1.5 mL microcentrifuge tube) were centrifuged for 20 min at 13000*g* (Eppendorf Centrifuge 5415D, Eppendorf North America, Westbury, NY). The supernatant was diluted to 0.05% (w/w). The protein contents in the supernatants were determined using a BCA Protein Assay Kit (Pierce Chemical Co., Rockford, IL). The solubility as a function of test time was calculated by eq 1, where $[concn]_0$ is the amount of bar at zero time (day 0) dissolved in PBS and $[concn]_t$ is the amount of bar at time t (stored for a period of time) dissolved in PBS:

$$\text{solubility (\%)} = \frac{[\text{concn}]_t}{[\text{concn}]_0} \times 100\% \quad (1)$$

Electrophoresis Analysis. Both sodium dodecyl sulfate−polyacrylamide gel electrophoresis (SDS-PAGE) and native-PAGE were performed using a Criterion Precast Gel System (two-gel Criterion cell). The above sample solutions (0.67%, w/w) were diluted to 0.05% (w/w) with the premixed Laemmli sample buffer or native sample buffer (Bio-Rad Laboratories Inc., Hercules, CA) and analyzed by SDS-PAGE as described by Laemmli (*22*) and by native-PAGE as described by Andrews (*23*), respectively. Criterion Precast gels (4−20% or 15% Tris-HCl gel, 18 well, Bio-Rad Laboratories) were used for both SDS-PAGE and native-PAGE analyses. Electrophoresis was run for 55 min at 200 V in a premixed electrophoresis running buffer: 10× Tris/glycine/SDS (Bio-Rad Laboratories Inc.) for SDS-PAGE and 10× Tris/glycine (Bio-Rad Laboratories Inc.) for native-PAGE. After electrophoresis, the gels were stained using a Coomassie stain kit (Biosafe, Bio-Rad Laboratories Inc.). The images of the destained gels were scanned on a scanner (Epson Perfection 4870, Epson America, Inc., Long Beach, CA). The densitometric analysis of band intensity was carried out on the Molecular Imager Gel Doc XR System (model Universal Hood II, Bio-Rad Laboratories Inc.) using the Quantity One 4.6.7 software program (Bio-Rad Laboratories Inc.).

Nature of Insoluble Materials. The sample suspension of WPI bars at day 28 dispersed in PBS as above (0.67% w/w, 1.5 mL × 3) was put into a 2 mL microcentrifuge tube and centrifuged for 20 min at 13000*g* (Eppendorf Centrifuge 5415D, Eppendorf North America). The supernatant was carefully removed by a sharp electrophoresis tip. This procedure was repeated three times to collect enough precipitate. Then PBS buffer (1.0 mL) was added to the precipitate in the tubes for washing. The tubes were vortexed on a vortex mixer to resuspend the precipitates, followed by centrifugation. The washing was repeated three times to remove any remaining soluble WPI proteins that might be attached to the precipitates. Each type of precipitate (i.e., insoluble aggregates) was individually resuspended in 1.0 mL of solvents, 5% SDS, 8 M urea, 8 M urea + 5% 2-ME, 5% SDS + 5% 2-Me, and left at room temperature overnight. After centrifuging at 13000*g* for 20 min, the supernatants were then subjected to SDS-PAGE analysis.

Scanning Electron Microscopy (SEM). The microstructure of the WPI bars was investigated using SEM. The specimens from the inside of the bars (to avoid the dried surface of the bars) were cut into cubes (~3 × 3 × 3 mm) with a stainless steel cutter. The specimens were soaked in glutaraldehyde (4%, in 0.1 M phosphate buffer at pH 7.2) for 3 days at 4 °C for fixation. After fixation, the specimens were rinsed with the 0.1 M phosphate buffer at pH 7.2 three times for times of 30, 90, and 120 min, respectively. The specimens were then further postfixed with OsO_2 (2%, in 0.1 M phosphate buffer at pH 7.2) for 1 h to prevent shrinkage of the structure that might occur during the dehydration. After rinsing with distilled water (three times for times of 30, 90, and 120 min, respectively), the specimens were dehydrated through a graded series of ethanol solutions (in increasing concentrations of 25, 50, 75, 95, 100, 100, and 100% in turn, 1 h for each case). The specimens were finally dried by critical point treatment with liquid CO_2 (Critical Point Dryer, Autosamdri-814, *tousimis* Research Corp., Rockville, MD).

Two types of microstructure were observed for WPI bars: (1) surface structure, in which the specimen after drying was affixed to an aluminum stub with two-sided adhesive tape; and (2) fracture structure, which was used to investigate the inner structure of the bars. The specimens after drying were further scored by a razor blade and then broken into two pieces by a pinsetter at room temperature. The surfaces of the fracture were examined in the same way as the surface structure. In all cases, the specimens were coated with gold using a sputter coater (model EMS-76M, Ernest F. Fullam Inc.) and observed using a Hitachi S-3500N scanning electron microscope with operation conditions at an accelerating voltage of 5 kV. Triplicates were done for each sample.

Statistical Analysis. The valid test of statistical significance between rate constants (k) or shelf life (days) for different WPI bars is to calculate the 95% confidence limits (CL) and determine if the ranges overlap. If they do not overlap, then the rate constants or shelf life is significantly different, as Kamman and Labuza (*24*) showed, as compared to an ANOVA.

RESULTS AND DISCUSSION

Water Activity (a_w) of WPI Bars during Storage. After overnight storage (18 h at 45 °C) for the first day after dough formation, it was considered that the WPI proteins in all bars had been hydrated and moisture migration reached an initial equilibrium because the a_w did not change for the bars between freshly made and after overnight storage. The change in a_w, an index of water mobility, reflects the physical properties of food products and sheds some light on the stability of a product. During subsequent storage for 35 days at 45 °C, the a_w slightly decreased from an initial average value of 0.972 to 0.961. The effect of this minor reduction ($\Delta a_w = 0.011$) on the physical and chemical properties of WPI bars was ignored in this study, although the decrease suggests either that there was further moisture migration into the protein powder particles or that the loss of moisture due to water evaporation at 45 °C occurred during storage.

Texture of WPI Bars. The force−distance plots of WPI bars at days 1 and 35 (storage at 45 °C) are illustrated in **Figure 1**. At day 1, with the penetration of the probe into the bars, a large increase in force at < 1 mm distance is observed for all bars. After that, the force remains unchanged until ~3 mm and then slightly increases before yield for bar Cys0 (curve a, **Figure 1A**); the force is unchanged until ~2 mm and then slowly increases before yield for bar Cys0.05 (curve b, **Figure 1A**); the force keeps increasing for bar Cys0.25 before the final yield at ~4.5 mm (curve c, **Figure 1A**); and the force remains unchanged before yield for the Nem2 bar (curve d, **Figure 1A**). This pronounced difference in the texture profile among bars suggests that the inherent structures of four kinds of bars at day 1 are different. This might be caused by the interaction forces, which vary among bars during dough formation. After 35 days of storage at 45 °C, the texture profiles were different for all of the bars (**Figure 1B**) in comparison with the bars at day 1 (**Figure 1A**). In **Figure 1B** (note the scale is 4-fold compared to day 1), bars Cys0 (curve a), Cys0.05 (curve b), and

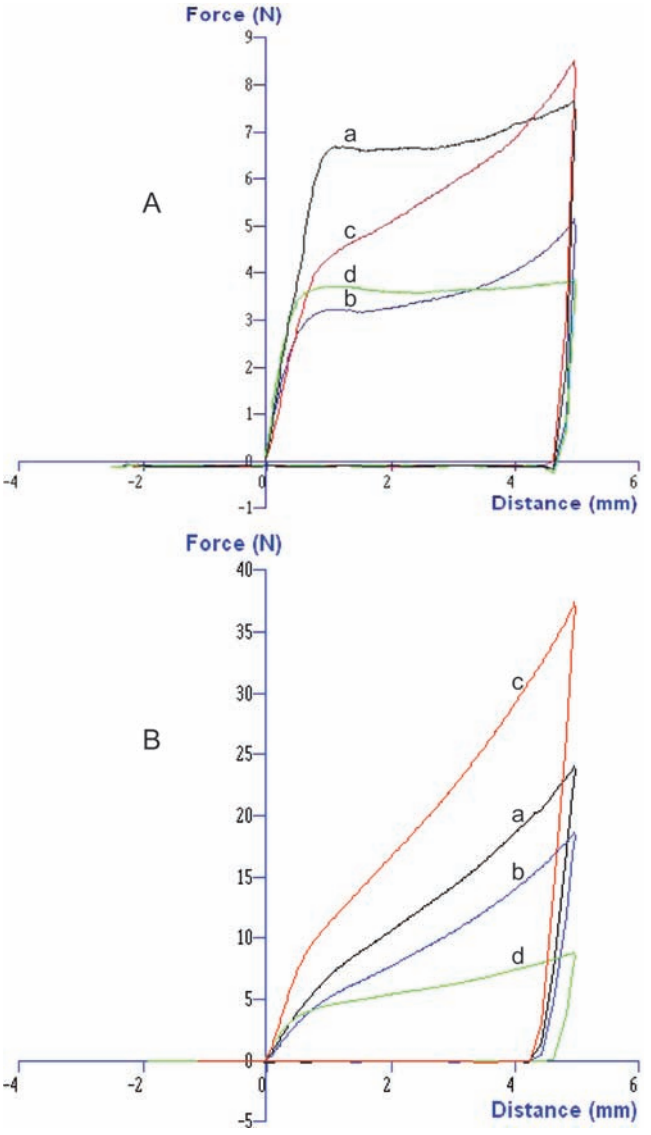

Figure 1. Texture profiles of WPI bars Cys0 (curve a), Cys0.05 (curve b), Cys0.25 (curve c), and Nem2 (curve d) at day 1 (**A**) and day 35 (**B**), as measured by a TA.XT PLUS texture analyzer.

Cys0.25 (curve c) show similar profiles, suggesting the similarity in the bar nature but to different degrees. After an initial increase (<1 mm distance as seen at day 1), the forces keep increasing, but the slopes (hardness increase/distance) are different for all bars, and it is in the order Nem2 < Cys0.05 < Cys0 < Cys0.25. Usually, the slope is an indication of the firmness of a food product. The higher the slope, that is, the Young's modulus, the firmer is the texture (*25*). In consideration with the results shown later, we assumed that the difference in the slopes or the firmness in four systems was mainly due to the differences in bar structures, which is the reflection of difference in the interaction forces. The slope of curve d in **Figure 1B** is very low and just slightly increased compared to curve d in **Figure 1A**. This indicates that bar Nem2 remained very soft and the interaction forces involved in the bar might be very weak ever after 35 days of storage at 45 °C.

Figure 2 shows the result of the bar hardness (force at 3 mm depth penetration) as a function of time at 45 °C. The force for all bars increases over time following a zero-order regression as indicated by straight lines in **Figure 2**. The kinetics of the results is shown in **Table 1**. The initial value of hardness by extrapolating the regression lines to zero time (day 0) is in the order Cys0.05

(3.0 N) < Nem2 (4.5 N) < Cys0.25 (4.8 N) < Cys0 (5.9 N) (**Table 1**). Compared with the control bar Cys0, the addition of Cys (WPI/Cys = 0.05) and NEM (WPI/NEM = 2) significantly and initially decreased the bar hardness, whereas the addition of Cys (WPI/Cys = 0.25) did not significantly decrease the bar hardness at the initial state. Similarly, the measured hardness of bars at day 1 follows the same order: Cys0.05 (4.2 N) < Nem2 (4.8 N) < Cys0.25 (5.5 N) < Cys0 (5.6 N) (**Table 1**). It was reported that WPI bar hardening in a WPI/buffer system was mainly due to the thiol−disulfide interchange reaction (*3*, *4*). After overnight hydration (18 h at 45 °C), the control bar (Cys0) underwent thiol−disulfide interchange reactions, resulting in a bar with a hardness of 5.8 N. Because Cys is able to weaken gels by cleaving and blocking further formation of disulfide bonds (*17*), we surmised that in the presence of Cys (WPI/Cys = 0.05), the disulfide bonds of WPI proteins were promptly cleaved, resulting in a hardness of 4.2 N at day 1, significantly softer than the control bar. For bar Cys0.25 (WPI/Cys = 0.25), the presence of a greater amount of Cys cuts the disulfide bonds, which results in unfolding of the proteins. If Cys could not immediately block the formation of new disulfide bonds, the thiol−disulfide interchange reaction might occur simultaneously. Thus, it produced a bar with a hardness of 5.6 N, which is not significantly different from the bar Cys0 (5.8 N). In the case of bar Nem2 (WPI/NEM = 2), the thiol−disulfide interchange reaction is completely inhibited by NEM, a thiol group blocking reagent, and the disulfide bonds of WPI proteins remain intact. As a consequence, bar Nem2 with a hardness of 4.8 N is significantly softer than the control bar but significantly harder than bar Cys0.05. These facts confirm that the thiol−disulfide interchange reaction occurs during dough formation and that the interaction forces vary depending on compositions. **Table 1** shows the rate constants for zero-order regression of hardness versus time are in the order Nem2 (0.05 N/day) < Cys0.05 (0.22 N/day) < Cys0 (0.23 N/day) < Cys0.25 (0.48 N/day). Compared to the control Cys0, the rate constant for bar Cys0.05 is not significantly different, whereas the rate constant for bar Cys0.25 is significantly increased. This suggests that, in comparison with the control Cys0, the thiol−disulfide interchange reaction during storage was not significantly reduced by the presence of Cys (WPI/Cys = 0.05), but it is significantly accelerated by an increase in Cys (WPI/Cys = 0.25). For the Nem2 bar, the increase in hardening with time is 5 times lower than that of the control. As seen in **Figure 2** the hardening increase over 35 days was not significant. The slight increase is probably caused by the noncovalent interactions, which are enhanced by the unfolding of the WPI protein molecules due to the attachment of NEM to the WPI proteins (*26*). This can result in the formation of a fibril network structure resulting from the intermolecular interactions, for example, the formation of β-sheets, as will be illustrated later in **Figure 8H**.

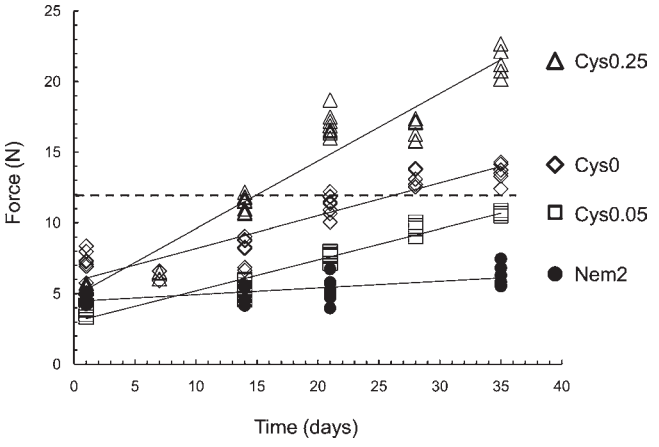

Figure 2. Hardness of WPI bars ($a_w \sim 0.97$) stored at 45 °C as a function of time. Straight lines are the linear regression curves.

The shelf-life time of bars is affected by both the initial state and the reaction rate. As judged by a panel's finger-touch test, which had been carried out in our laboratory, when protein bar hardness is > 12 N, the bar texture is very hard and is considered to be unacceptable. Note that these were not taste tested because of the addition of sodium azide. By this standard, as shown in **Table 1**, the control Cys0 has a shelf life of 26 days. Compared with the control, the shelf-life time was significantly extended by Cys0.05 (41 days) or Nem2 (161 days), but significantly shortened by Cys0.25 (15 days). In all cases the 95% confidence limits were not overlapping, so all were significantly different.

Solubility of WPI Bars in Buffer. The solubility of WPI bars in PBS was investigated to evaluate the loss of protein quality due to the formation of insoluble materials during storage. The semilog plot of the solubility of WPI bars as a function of time is shown in **Figure 3**. The kinetics of solubility follows a first-order regression as summarized in **Table 2**. Assuming that protein solubility is 100% (pH > 6) before mixing (*3*, *4*, *7*), the measured degrees of solubility at day 1 were 91, 85, 71, and 98% for bars Cys0, Cys0.05, Cys0.25, and Nem2, respectively. The data obtained by first-order regression show that the initial value of solubility at day 0 was ~100% for bar Nem2, indicating almost no loss of solubility; these values were ~84% for Cys0 and Cys0.05 and ~67% for Cys0.25, significant decreases in solubility. The rapid decrease of solubility with increasing amount of Cys at day 0 suggested that both the thiol−disulfide interchange reaction and hydrophobic interactions occur as soon as the hydration starts. The increased loss of solubility is probably due to the further hydrophobic interaction. The addition of Cys breaks down disulfide bonds, leading to the unfolding of peptides, thus promoting the formation of insoluble materials via hydrophobic interaction. In **Figure 3**, solubility decreased with time in all systems with Nem2 showing the least decrease and Cys0.25 the greatest. Compared to the rate constant for the loss of solubility for Cys0 (0.020 day^{-1}), the rate of loss of solubility after day 1 was not significantly decreased for Cys0.25 (0.016 day^{-1}) but was significantly for Cys0.25 (0.015 day^{-1}), whereas Nem2 (0.0085 day^{-1})

Table 1. Kinetics of WPI Bar Hardening by Zero-Order Regression (Bars Were Stored at 45 °C, $a_w \sim 0.97$, $n = 3$)

	hardness (N)		rate constant (N/day)		
WPI bar	measured value at day 1 ± SD	initial value[a] (L, U)[b]	k (L, U)[b]	R^2	time to 12 N (days) (L, U)[b]
Cys0	5.8 ± 1.8	5.9 (5.2, 6.5) a	0.23 (0.20, 0.26) a	0.85	26 (30, 23) a
Cys0.05	4.2 ± 0.8	3.0 (2.5, 3.5) b	0.22 (0.20, 0.24) a	0.93	41 (46, 37) b
Cys0.25	5.6 ± 0.9	4.8 (4.0, 5.6) ac	0.48 (0.44, 0.52) b	0.94	15 (16, 14) c
Nem2	4.8 ± 0.5	4.5 (4.0, 4.9) c	0.05 (0.02, 0.07) c	0.43	161 (299, 110) d

[a] Initial value: zero-order intercept obtained by extrapolating regression curve to day 0. Letters a−d indicate significance: the same letter indicates no significant difference at $p < 0.05$ level. [b] L, lower 95% CL; U, upper 95% CL.

had a rate < 50% of the control. Using 50% loss of solubility as an index for judging deterioration of bar quality, the times to reach 50% loss of solubility are significantly different, and they are in the order Cys0.25 (18 days) < Cys0 (26 days) < Cys0.05 (35 days) < Nem2 (85 days) (**Table 2**). Note that even though the rate of loss for Cys0.25 is not significantly slower than the control, it has the greatest initial loss of solubility (33%) at day 1, and so the shortest shelf life, whereas the Cys0.05 gave a 25% increase in shelf life due to significant slowing of the loss of solubility. During storage, also both the thiol−disulfide interchange reaction and hydrophobic interaction contributed to the formation of insoluble materials. This is because the extent of both covalent and noncovalent interactions during storage depends on the gradual unfolding of WPI molecules. The decreased loss of solubility for the Nem2 bar can be attributed to the sole hydrophobic interaction due to the blocking of the free thiol group by NEM (*26*). The unfolding of WPI molecules is slower than other systems. Thus, the rate constant of the Nem2 bar for the loss of solubility is significantly slower than those of the other bars, therefore indicating the longest shelf life (85 days).

The difference of shelf life between the days to 50% loss of solubility (**Table 2**) and the days to a hardness of 12 N (**Table 1**) is ~0 day for Cys0, ~ −6 days for Cys0.05, ~ +3 days for Cys0.25, and ~ −75 days for Nem2. This discrepancy is likely due to an increase of hydrophobic interactions between hydrophobic amino acid residues when exposed in the polar buffer solution, causing further loss of solubility. For example, for Cys0.05, the cleavage of disulfide bonds by Cys should unfold the α-la (*17*), whereas the attachment of NEM to proteins would unfold the *β*-lg structure (*26*).

Electrophoresis Analysis. To further understand the proposed interaction forces involved in bar hardening, native-PAGE and nonreducing and reducing SDS-PAGE of the samples dispersed in PBS were performed, as shown in **Figure 4**. The identification of bands was carried out by running samples with a molecular weight standard, untreated WPI, and comparing the results with the literature (*27*). Only the effects of α-la and *β*-lg, which account for 91% of the WPI proteins, is discussed in this context.

Regardless of the presence of Cys, on native-PAGE (**Figure 4A**) the band intensity of both α-la and *β*-lg markedly decreased with time with the appearance of aggregates on the top of the gel. On nonreducing SDS-PAGE (**Figure 4B**), the decrease of band intensity with time is obvious for α-la but less obvious for *β*-lg, whereas aggregates are still observable on the top of the gel. There is no doubt that noncovalent interactions are involved in the

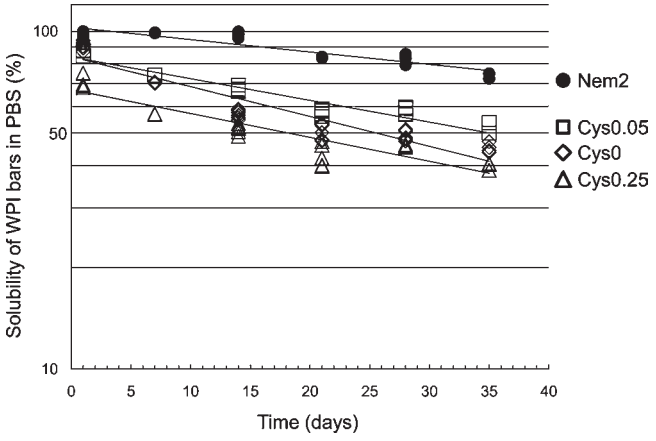

Figure 3. Semilog plot of the solubility of WPI bars in PBS as a function of time (bars were stored at 45 °C, a_w ~0.97, n = 3). Straight lines are the linear regression curves.

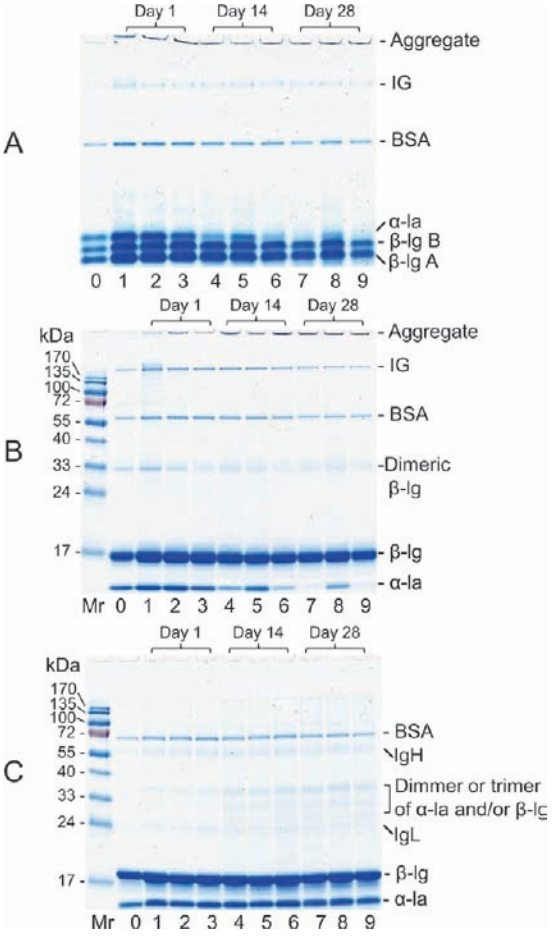

Figure 4. Native-PAGE (**A**), nonreducing SDS-PAGE (**B**), and reducing SDS-PAGE (**C**) of the dispersions of WPI bars (45 °C) in PBS: lane 0, untreated WPI; lanes 1−3, at day 1; lanes 4−6, at day 14; lanes 7−9, at day 28. Lanes 1, 4, and 7 are bars with Cys0; lanes 2, 5, and 8 are bars with Cys0.05; lanes 3, 6, and 9 are bars with Cys0.25. IG, immunoglobulin; IgH, IgL, heavy and light immunoglobulin fractions; M_r, molecular weight marker. 15% gel.

Table 2. Kinetics of the Loss of Solubility by First-Order Regression (Bars Were Stored at 45 °C, a_w ~ 0.97, n = 3)

	solubility (%)		rate constant (day^{-1}) for loss		
WPI bar	measured solubility at day 1 ± SD	initial solubility [a] (L, U)[b]	k (L, U)[b]	R^2	time to 50% loss of solubility (days) (L, U)[b]
Cys0	91 ± 3	84 (79, 90) a	0.020 (0.024, 0.017) a	0.87	26 (22, 30) a
Cys0.05	85 ± 2	84 (81, 87) a	0.015 (0.016, 0.013) b	0.93	35 (31, 39) b
Cys0.25	71 ± 3	67 (63, 71) b	0.016 (0.019, 0.014) ab	0.84	18 (15, 22) c
Nem2	98 ± 2	100 (99, 100) c	0.008 (0.010, 0.006) c	0.81	85 (69, 112) d

[a] Initial value: first-order intercept obtained by extrapolating regression curve to day 0. Letters a−d indicate significance: the same letter indicates no significant difference at $p < 0.05$ level. [b] L, lower 95% CL; U, upper 95% CL.

Table 3. Relative Intensity of Bands of WPI Bars on Native-PAGE and Nonreducing SDS-PAGE (Bars Were Stored at 45°C, $a_w \sim 0.97$, $n = 3$)

		native-PAGE			nonreducing SDS-PAGE		
band	time	Cys0	Cys0.05	Cys0.25	Cys0	Cys0.05	Cys0.25
α-la	day 1	100	92	76	100	100	78
	day 14	50	67	33	48	75	44
	day 28	22	36	20	23	67	15
β-lg	day 1	100	95	89	100	99	98
	day 14	78	76	69	93	97	92
	day 28	67	70	51	84	92	79

formation of aggregates. The bands of both α-la and β-lg, irrespective of time, show almost identical intensity on reducing SDS-PAGE, and no aggregates stayed on the top of the gel (**Figure 4C**), implying that all of the disulfide bonds in aggregates induced by the thiol−disulfide interchange reaction were broken down by 2-Me. These facts indicate that for bars Cys0, Cys0.05, and Cys0.25, both α-la and β-lg were involved in the formation of insoluble materials through the thiol−disulfide interchange reaction as well as noncovalent interactions, and both interaction forces are time-dependent. A number of new bands with molecular weights of ∼28−36 kDa, which appeared to be the dimers or trimers of α-la and/or β-lg, were observed only upon using the reducing SDS-PAGE (**Figure 4C**). The formation of these new species was also time-dependent. Considering the formation of a fibril structure in all bars (**Figure 8**), we boldly speculated that the force might be "enhanced" noncovalent interactions including both hydrophobic interactions and hydrogen bonding. However, this needs to be confirmed. The relative intensities of bands on the native-PAGE and nonreducing SDS-PAGE was further estimated by densitometric analysis (the method error is ∼5%) and are shown in **Table 3**. On day 28, the band intensity of β-lg, which accounts for 64% of the WPI proteins (*20*), was decreased by 33% in the control Cys0, by 30% for Cys0.05, and by 49% for Cys0.25 on native-PAGE and by 16% for the control Cys0, by 8% for Cys0.05, and by 21% for Cys0.25 on nonreducing SDS-PAGE. Apparently, for β-lg, both noncovalent interactions and thiol−disulfide interchange reaction are involved in all bars. The effect of noncovalent interactions slightly increased in the order Cys0 < Cys0.05 < Cys0.25, whereas the effect of thiol−disulfide interchange reaction is in the order Cys0.05 < Cys0 < Cys0.25. The band intensity of α-la (day 28), which accounts for 27% of the WPI proteins (*20*), reduced to 22% for Cys0, to 36% for Cys0.05, and to 20% for Cys0.25 on native-PAGE and to 23% for Cys0, to 67% for Cys0.05, and to 15% for Cys0.25 on nonreducing SDS-PAGE. For α-la, the effect from noncovalent interactions was not as obvious in Cys0 and Cys0.25 but evidently observed in Cys0.05. The involvement of thiol−disulfide interchange reactions from α-la in all bars was prominent, and the reaction extent was in the order Cys0.05 < Cys0 < Cys0.25. Apparently, the α-la in the control bar (Cys0) and bar Cys0.25 is mainly incorporated into the insoluble materials via the thiol−disulfide interchange reaction, whereas the α-la in the bar Cys0.05 was aggregated into the insoluble materials through both thiol−disulfide interchange reaction and noncovalent interactions. Overall, compared with the control (Cys0), Cys0.05 slowed, whereas Cys0.25 accelerated, the thiol−disulfide interchange reaction of both α-la and β-lg. These results are in agreement with the observations from texture and solubility analyses. From the relative composition of β-lg and α-la in WPI as well as the percentage disappearance of the two proteins during 28 days of storage at 45 °C, as illustrated by nonreducing and reducing SDS-PAGE, the incorporation of α-la via the thiol−disulfide interchange reaction into the insoluble

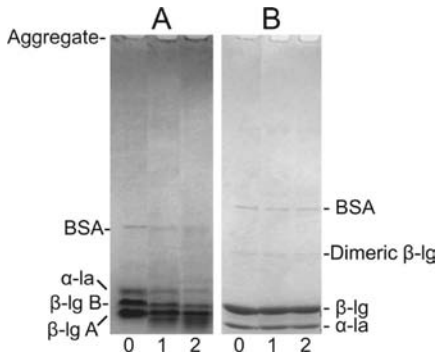

Figure 5. Native-PAGE (**A**) and nonreducing SDS-PAGE (**B**) of the dispersions of bar Nem2 in PBS (45 °C) at day 1 (lane 1) and day 28 (lane 2). Lane 0 is untreated WPI used as marker. 4−20% gel.

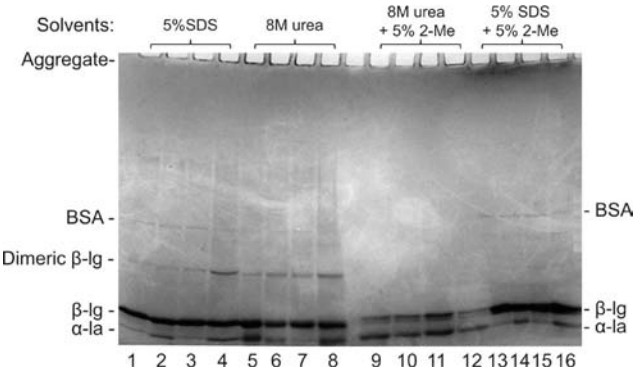

Figure 6. SDS-PAGE of insoluble aggregates from bars Cys0 (lanes 1, 5, 9, and 13); Cys0.05 (lanes 2, 6, 10, and 14); Cys0.25 (lanes 3, 7, 11, and 15); and Nem2 (lanes 4, 8, 12, and 16) dissolved in 5% SDS (lanes 1−4, 6 μg of WPI/lane); 8 M urea (lanes 5−8, 6 μg of WPI/lane); 8 M urea + 5% 2-ME (lanes 9−12, 2 μg of WPI/lane); and 5% SDS + 5% 2-Me (lanes 13−16, 6 μg of WPI/lane). The WPI bars were stored for 28 days at 45 °C. 4−20% gel.

materials is greater than that of β-lg. The α-la has no free thiol group and has four disulfides, whereas β-lg has one free thiol group and two disulfide bonds. It has been reported that when heated at 75 °C on its own, α-la did not form aggregates, whereas β-lg formed large aggregates. The two proteins interacted to form soluble aggregates as well as larger particles through both disulfide bonds and hydrophobic interactions (*5*, *28*). The aggregation rate of α-la increased when heated in combination with β-lg (*29*). It is possible that the thiol−disulfide interchange reaction also occurred between α-la and β-lg for the WPI bars during storage at 45 °C. On the basis of the data in **Table 3**, the molar ratios of the loss of α-la and β-lg at day 28, that is, the molar ratio of the two proteins that were merged into aggregates by the thiol−disulfide interchange reaction, were 6.2 (Cys0), 5.7 (Cys0.05), and 5.1 (Cys0.25), respectively. In the presence of Cys, the cleavage and blocking of Cys to the disulfide bonds on α-la molecules reduced the reactivity/extent of α-la to aggregate as compared with the control Cys0.

For the Nem2 bar, the band intensity of α-la and β-lg B decreased with time; meanwhile, some aggregates stopped on the top of the gel on the native-PAGE (lanes 1−2, **Figure 5A**). On the nonreducing SDS-PAGE (lanes 1−2, **Figure 5B**), all of the bands of both α-la and β-lg showed identical intensity and aggregates disappeared from the top of the gel, indicating that the insoluble materials from the Nem2 bar are caused by noncovalent interactions. The bands of β-lg A were smeared at both day 1 and day 28

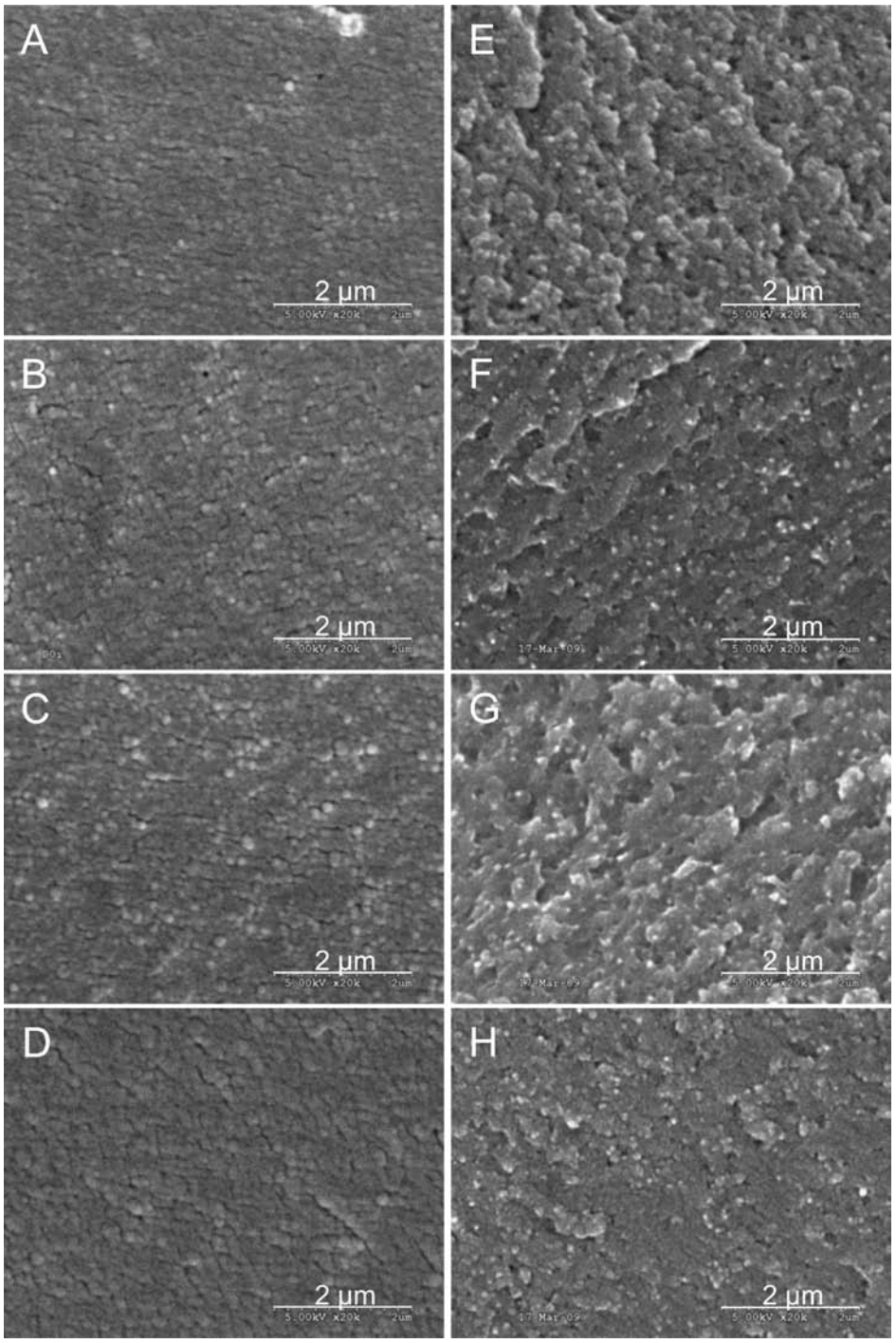

Figure 7. Fracture images of WPI bar specimen: Cys0 (**A**, **E**); Cys0.05 (**B**, **F**); Cys0.25 (**C**, **G**); and Nem2 (**D**, **H**) were bars at day 1 (**A**−**D**) and day 28 (**E**−**H**) at 45 °C. The original magnifications were ×20K.

on native-PAGE (lanes 1−2, **Figure 5A**). This is probably due to the covalent attachment of NEM to the free thiol group of β-lg, which unfolds the β-lg molecule (mainly β-lg A) and also changes the distribution of charge density, leading to smeared bands (*26*). It is known that NEM binds rapidly and specifically to free thiol groups (*30*). The blocking of the thiol group of β-lg gave a protein derivative that would not aggregate via disulfide interchange reactions but can be aggregated by nonspecific interaction forces (*31*). Clearly, for Nem2, it is only the noncovalent interactions that resulted in the formation of insoluble materials and, therefore, bar hardening.

Nature of Insoluble Materials. To further understand the nature of the insoluble materials formed during storage, the precipitates from the WPI bars (stored for 28 days at 45 °C) were examined by dissolving them in different solvents as described under Materials and Methods. All precipitates from Cys0, Cys0.05, and Cys0.25 were ~4% dissolved in the solvents 5% SDS and 5% SDS + 5% 2-Me, forming a milky white opaque suspension. A slightly higher percentage of the precipitates (~16%, for each of the bar systems) dissolved in 8 M urea with a clear solution for the dissolved portion and a precipitate for undissolved portion. All of the precipitates were quickly dissolved in 8 M urea + 5% 2-Me solvent with clear solutions. The precipitate from Nem2 rapidly dissolved in all four solvents. These results are expected because 8 M urea, which disperses both hydrophobic interactions and hydrogen bonding, is a much more powerful solvent than 5% SDS, which

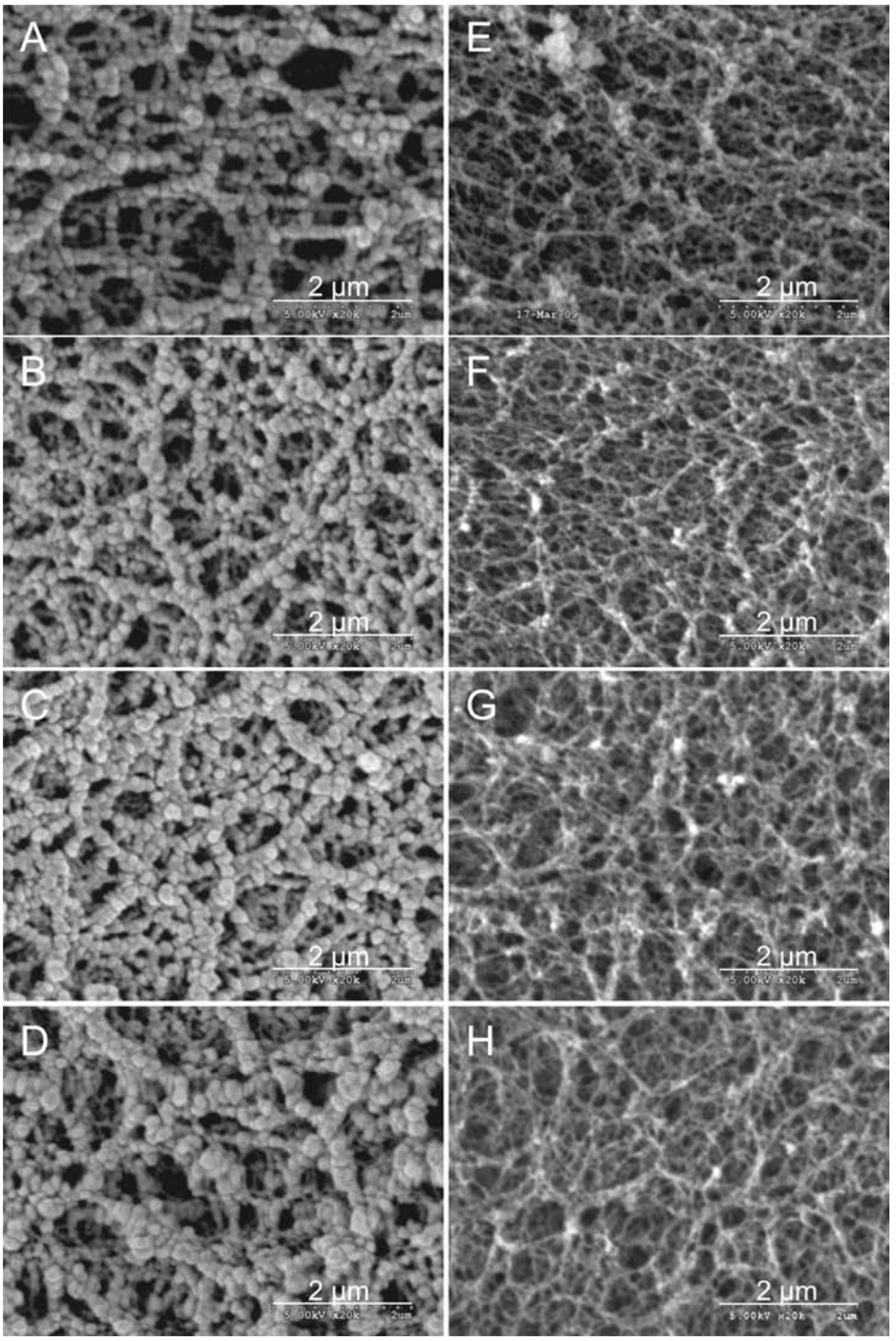

Figure 8. Surface images of WPI bar specimen: Cys0 (**A**, **E**); Cys0.05 (**B**, **F**); Cys0.25 (**C**, **G**); and Nem2 (**D**, **H**) were bars at day 1 (**A**−**D**) and day 28 (**E**−**H**) at 45 °C. The original magnifications were ×20K.

disperses only hydrophobic interactions. The 8 M urea + 5% 2-Me solvent is the most powerful in disrupting the noncovalent interactions and breaking down disulfide bonds. The solvent 5% SDS + 5% 2-Me did not improve the solubility of the precipitates compared to 5% SDS. This is perhaps due to the weak interaction of 5% SDS, which could not dissolve aggregates and/or unfold the protein peptides, so that 2-Me could not enter the inside of the precipitates to break down the disulfide bonds.

The SDS-PAGE analysis of the supernatants after centrifugation is shown in **Figure 6**. As viewed, the band intensities of β-lg (lanes 1−4, **Figure 6**) were very similar, indicating that the β-lg, which was dissolved from all of the bars by 5% SDS to almost equal extents, was associated into the aggregates by noncovalent interactions during mixing and storage at 45 °C. As far as α-la is concerned, more α-la was dissolved in 5% SDS from the Cys0.05 and Nem2 bars (lanes 2 and 4, **Figure 6**) than from the Cys0 and Cys0.25 bars (lanes 1 and 3, **Figure 6**). This indicates that a portion of α-la from Cys0.05 and Nem2 was associated by noncovalent interactions, but not that much for Cys0 and Cys0.25. The relative band intensity of α-la from Cys0.05 is stronger in 8 M urea + 5% 2-Me (lane 10, **Figure 6**) than in other solvents (lanes 2, 6, and 14, **Figure 6**), meaning that α-la was also dissociated from the aggregates by breaking disulfide bonds in the presence of 2-Me. For the control bar (Cys0), the band intensity of α-la in 8 M urea (lane 5, **Figure 6**) is stronger than in 5% SDS (lane 1, **Figure 6**) or 5% SDS + 5% 2-Me (lane 13, **Figure 6**), showing that more α-la

was dissociated from the aggregates through interrupting noncovalent interactions by 8 M urea than by 5% SDS or by 5% SDS + 5% 2-Me. In the case of bar Cys0.25, the band intensity of α-la is very faint in solvents 5% SDS, 8 M urea, and 5% SDS + 5% 2-Me (lanes 3, 7, and 15, **Figure 6**), but it is very dense in 8 M urea + 5% 2-Me (lane 11, **Figure 6**), indicating that the α-la in bar Cys0.25 was primarily associated into the aggregates by thiol−disulfide interchange reaction. The amounts of α-la and β-lg found in the insoluble aggregates as shown in **Figure 6** (lanes 9−11) were not in correspondence with the amount lost in **Table 3** because, in 8 M urea + 5% 2-Me solvent, the insoluble aggregates dissociated into not only α-la and β-lg but also some adducts of α-la and βlg as clearly indicated in **Figure 4C**. It is interesting to note that the relative ratio of band intensities of the dissolved aggregates in 5% SDS or 8 M urea was α-la < β-lg (lanes 1−3 and 5−7, **Figure 6**), whereas it became α-la > β-lg (lanes 9−11, **Figure 6**) when dissolved in 8 M urea + 5% 2-Me. Apparently, β-lg was more responsible for the aggregation via noncovalent interactions than α-la, whereas α-la is more responsible for the aggregation caused by the thiol−disulfide interchange reaction than β-lg. These results from SDS-PAGE analysis (**Figures 4** and **6**) led us to deduce that the free thiol group on β-lg initiated the thiol−disulfide interchange reaction but further polymerization was favored for α-la.

From the above, it is clear that insoluble materials from all bars were mainly composed of both β-lg and α-la. The β-lg was mainly associated into the aggregates through noncovalent interactions for all bars, whereas α-la mainly was incorporated through the thiol−disulfide interaction and was in the order Cys0.05 < control (Cys0) < Cys0.25 (except Nem2). The analysis from the insoluble materials further confirmed that the presence of the appropriate amount of cysteine (Cys/WPI = 0.05) reduced the thiol−disulfide interaction caused by α-la. These results were consistent with the results obtained by analyzing the sample solutions dispersed in PBS.

Microstructure of WPI Bars by SEM. The microstructure of the WPI bars at days 1 and 28 at 45 °C was observed by SEM as shown in **Figures 7** (fracture image) and **8** (surface image). Using the treatment as described under Materials and Methods, the fracture image of the specimen (**Figure 7**) reflects the interior structure of the specimen in which glutaraldehyde, OsO_2, and ethanol could not penetrate into the interior of the specimen with no change in moisture. The surface image of the specimen (**Figure 8**) reflects the protein structures from which sample moisture was removed by ethanol.

The fracture images show that all bars at day 1 appear to be similarly smooth with very tiny granules with a size of 0.1−0.2 μm (**Figure 7A−D**). After being stored for 28 days at 45 °C, the texture of the bars became coarse with large lumps (**Figure 7E−H**). The roughness appears in the order Nem2 < Cys0.05 < Cys0 ∼ Cys0.25. As discussed earlier, the loss of solubility of the bars was in the order Nem2 (18%) < Cys0.05 (42%) < Cys0 (51%) < Cys0.25 (54%). It is assumed that the degree of the roughness/lumps is related to the formation of insoluble aggregates. The surface structure shows that the proteins in all of the bars appear to align into a beaded string structure at day 1 (**Figure 8A−D**). The beads have an average thickness ∼25−30 nm. At day 28, all of the bars developed into a smooth, thin-thread dense cross-linked network structure (**Figure 8E−H**). This microstructural network is similar to that of whey protein gels as observed by Langton and Hermansson (*32*). The thickness of the strand is ∼10 nm in diameter. Visually, structural alignment occurred at day 1 (the bars were stored for ∼18 h at 45 °C). This might be due to the high concentration of WPI in the bars (60% WPI). The transition of the structure from the beaded string structure at day 1 into the thin-smooth fibril structure at day 28 suggests that the rearrangement of the structure evolves with time as a result of the interaction forces involved, like the formation of many amyloid-like fibrils as reported (*33*, *34*). As discussed above, both the noncovalent interactions and the thiol−disulfide interchange reaction are involved in protein aggregation in the bars (Cys0; Cys0.05; Cys0.25). The same structural changes are observed for the bars in the presence of NEM (Nem2), which includes only noncovalent interactions. Evidently, the formation of these fibril structures resulting from the rearrangement in all of the bars was mainly due to noncovalent interactions (*33*, *34*). Considering that the bar in the presence of NEM also hardened after much longer storage at 45 °C and that for the bars in the absence of NEM thiol−disulfide interchange reactions should have reached equilibrium during storage, it is tempting to assume that the noncovalent interactions, resulting in the fibril network structure, would dominate the hardness of bars in long-term storage.

In conclusion, WPI protein bars in model systems harden with time (ASLT, 45 °C). Bar hardening is due to the formation of insoluble aggregates induced by the thiol−disulfide interchange reaction and/or noncovalent interactions. The structural rearrangement of protein aggregates also plays an important role in bar hardening. Compared with the control bar Cys0 (shelf-life time ∼26 days based on time to 12 N), an appropriate addition of Cys (WPI/Cys = 0.05) significantly extended the bar shelf-life time by ∼14 days by delaying the thiol−disulfide interchange reaction of α-la; an excess addition of Cys (WPI/Cys = 0.25) significantly shortens the bar shelf-life time by 11 days by accelerating the thiol−disulfide interchange reaction; and the bar in the presence of NEM (WPI/NEM = 2) has a 6-fold longer shelf-life time because only noncovalent interactions are occurring between the proteins.

LITERATURE CITED

(1) Brown, E. C.; DiSilvestro, R. A.; Babaknia, A.; Devor, S. T. Soy versus whey protein bars: effects on exercise training impact on lean body mass and antioxidant status. *Nutr. J.* **2004**, *3*, 22–26.

(2) Most, M. M.; Miller, D. L.; Redmann, S.; Greenway, F.; Lefevre, M. Nutrition bar containing ingradients beneficial for heart health improves LDL-cholesterol levels. *J. Am. Diet. Assoc.* **2006**, *106*, A23–23.

(3) Zhou, P.; Liu, X.-M.; Labuza, T. P. Moisture-induced aggregation of whey proteins in a protein/buffer model system. *J. Agric. Food Chem.* **2008**, *56*, 2048–2054.

(4) Zhou, P.; Liu, X.-M.; Labuza, T. P. Effects of moisture-induced whey protein aggregation on protein conformation, the state of water molecules, and the microstructure and texture of high-protein-containing matrix. *J. Agric. Food Chem.* **2008**, *56*, 4534–4540.

(5) Dalgleish, D. G.; Senaratne, V.; Francois, S. Interactions between α-lactalbumin and β-lactoglobumin in the early stages of heat denaturation. *J. Agric. Food Chem.* **1997**, *45*, 3459–3464.

(6) Bell, L. N.; Labuza, T. P. Influence of the low-moisture state on pH and its implication for reaction kinetics. *J. Food Eng.* **1994**, *22*, 291–312.

(7) Zhu, D.; Damodaran, S.; Lucey, J. A. Physicochemical and emulsifying properties of whey protein isolate (WPI)−dextran conjugates produced in aqueous solution. *J. Agric. Food Chem.* **2010**, *58*, 2988–2994.

(8) Labuza, T. P.; Massaro, S. A. Browning and amino acid loss in model total parenteral nutrition solutions. *J. Food Sci.* **1990**, *55*, 821–826.

(9) Li, M.; Lee, T.-C. Effect of cysteine on the functional properties and microstructures of wheat flour extrudates. *J. Agric. Food Chem.* **1996**, *44*, 1871–1880.

(10) Watanabe, Y.; Horii, I.; Nakayama, Y.; Osawa, T. Effect of cysteine on bovine serum albumin (BSA) denaturation induced by solar ultraviolet (UVA, UVB) irradiation. *Chem. Pharm. Bull.* **1991**, *39*, 1796–1801.

(11) Huggins, C.; Tapley, D. F.; Jensen, E. V. Sulphydryl−disulphide relationships in the induction of gels in proteins by urea. *Nature* **1951**, *167*, 592–593.

(12) Frensdorff, H. K.; Watson, M. T.; Kauzmann, W. The kinetics of protein denaturation. V. The viscosity of urea solutions of serum albumin. *J. Am. Chem. Soc.* **1953**, *75*, 5167–5162.
(13) Schmidt, R. H.; Illingworth, B. L.; Ahmed, E. M. Heat-induced gelation of peanut protein/whey protein blends. *J. Food Sci.* **1978**, *43*, 613–621.
(14) Schmidt, R. H.; Illingworth, B. L.; Deng, J. C.; Cornell, J. A. Multiple regression and response surface analysis of the effects of calcium chloride and cysteine on heat-induced whey protein gelation. *J. Agric. Food Chem.* **1979**, *27*, 529–532.
(15) Furukawa, T.; Ohta, S. Mechanical and water-holding properties of heat-induced soy protein gels as related to their structural aspects. *J. Texture Stud.* **1982**, *13*, 59–69.
(16) Arntfield, S. D.; Murray, E. D.; Ismond, M. A. H. Role of disulfide bonds in determining the rheological and microstructural properties of heat-induced protein networks from ovalbumin and vicilin. *J. Agric. Food Chem.* **1991**, *39*, 1378–1385.
(17) Wang, C.-H.; Damodaran, S. Thermal gelation of globular proteins: weight-average molecular weight dependence of gel strength. *J. Agric. Food Chem.* **1990**, *38*, 1157–1164.
(18) Li, M.; Lee, T.-C. Effect of cysteine on the molecular weight distribution and the disulfide cross-link of wheat flour proteins in extrudates. *J. Agric. Food Chem.* **1998**, *46*, 846–853.
(19) Dreese, P. C.; Faubion, J. M.; Hoseney, R. C. Dynamic rheological properties of flour, gluten, and gluten-starch doughs. II. Effect of various processing and ingredient changes. *Cereal Chem.* **1988**, *65*, 354–359.
(20) Zhu, H.; Damodaran, S. Proteose peptones and physical factors affect foaming properties of whey protein isolate. *J. Food Sci.* **1994**, *59*, 554–560.
(21) Fairley, P.; Monahan, F. J.; German, J. B.; Krochta, J. M. Mechanical properties and water vapor permeability of edible films from whey protein isolate and *N*-ethylmaleimide or cysteine. *J. Agric. Food Chem.* **1996**, *44*, 3789–3792.
(22) Laemmli, U. K. Cleavage of structural protein during the assembly of the head of bacteriophage T4. *Nature* **1970**, *227*, 680–685.
(23) Andrews, A. T. Proteinases in normal bovine milk and their action on caseins. *J. Dairy Res.* **1983**, *50*, 45–55.
(24) Labuza, T. P.; Kamman, J. F. Reaction kinetics and accelerated test simulation as a function of temperature. In *Applications of Computers in Food Research and Food Industry*; Saguy, I., Ed.; Dekker: New York, 1983; pp 71−151.
(25) Bounce, M. C. In *Book Food Texture and Viscosity: Concept and Measurement*, 2nd ed.; Academic Press: New York, 2002.
(26) Wada, R.; Fujita, Y.; Kitabatake, N. Effects of heating at neutral and acid pH on the structure of β-lactoglobulin A revealed by differential scanning calorimetry and circular dichroism spectroscopy. *Biochim. Biophys. Acta* **2006**, *1760*, 841–847.
(27) Hwang, D.-C.; Damodaran, S. Selective precipitation and removal of lipids from cheese whey using chitosan. *J. Agric. Food Chem.* **1995**, *43*, 33–37.
(28) Schokker, E. P.; Singh, H.; Creamer, L. K. Heat-induced aggregation of β-lactoglobulin A and B with α-lactalbumin. *Int. Dairy J.* **2000**, *10*, 843–853.
(29) Hines, M. E.; Foegeding, E. A. Interactions of α-lactalbumin and bovine serum albumin with β-lactoglobulin in thermally induced gelation. *J. Agric. Food Chem.* **1993**, *41*, 341–346.
(30) Xiong, Y. L.; Kinsella, J. E. Mechanism of urea-induced whey protein gelation. *J. Agric. Food Chem.* **1990**, *38*, 1887–1891.
(31) Sawyer, W. H. Heat denaturation of bovine β-lactoglobulins and relevance of disulfide aggregation. *J. Dairy Sci.* **1968**, *51*, 323–329.
(32) Langton, M.; Hermansson, A.-M. Fine-stranded and particulate gels of β-lactoglobulin and whey protein at varying pH. *Food Hydrocolloids* **1992**, *5*, 523–539.
(33) Chiti, F.; Taddei, N.; Baroni, F.; Capanni, C.; Stefani, M.; Ramponi, G.; Dobson, C. M. Kinetic partitioning of protein folding and aggregation. *Nat. Struct. Biol.* **2002**, *9*, 137–143.
(34) Hamada, D.; Dobson, C. M. A kinetic study of β-lactoglobulin amyloid fibril formation promoted by urea. *Protein Sci.* **2002**, *11*, 2417–2426.

Received for review February 23, 2010. Revised manuscript received May 22, 2010. Accepted June 1, 2010. This project is funded by the USDA National Research Initiative (NRI, Grant 2007-35503-18406). Earlier work that was funded by Dairy Marketing Inc. led to the USDA NRI grant and must also be recognized. We thank Davisco Foods International, Inc., for financial support.